Temperature-Transferable Coarse-Grained Potentials for Ethylbenzene, Polystyrene, and Their Mixtures

Hu-Jun Qian,*,† Paola Carbone,†,§ Xiaoyu Chen,† Hossein Ali Karimi-Varzaneh,† Chee Chin Liew,‡ and Florian Müller-Plathe†

Eduard-Zintl-Institut für Anorganische and Physikalische Chemie, Technische Universität Darmstadt, Petersenstrasse 20, D-64287 Darmstadt, Germany, Polymer Research, BASF SE, D-67056 Ludwigshafen, Germany, and School of Chemical Engineering and Analytical Science, University of Manchester, P.O. Box 88, Sackville Street, Manchester M60 1QD, U.K.

Received August 22, 2008; Revised Manuscript Received October 30, 2008

ABSTRACT: In this article, we present coarse-grained potentials of ethylbenzene developed at 298 K and of amorphous polystyrene developed at 500 K by the pressure-corrected iterative Boltzmann inversion method. The potentials are optimized against the fully atomistic simulations until the radial distribution functions generated from coarse-grained simulations are consistent with atomistic simulations. In the coarse-grained polystyrene melts of different chain lengths, the Flory exponent of 0.58 is obtained for chain statistics. Both potentials of polystyrene and ethylbenzene are transferable over a broad range of temperature. The thermal expansion coefficients of the fully atomistic simulations are well reproduced in the coarse-grained models for both systems. However, for the case of ethylbenzene, the coarse-grained potential is temperature-dependent. The potential needs to be modified by a temperature factor of $\sqrt{T/T_0}$ when it is transferred to other temperatures; $T_0 = 298$ K is the temperature at which the coarse-grained potential has been developed. For the case of polystyrene, the coarse-grained potential is temperature-independent. An optimum geometrical combination rule is proposed with the combination constant $x = 0.4$ for mutual interactions between the polystyrene monomer and ethylbenzene molecules in their mixtures at different composition and different temperature.

1. Introduction

The broad span of time and length scales in biosystems and material science is a challenge for computer simulation and modeling. In the field of polymers, there are many simulation techniques and models that vary from the atomistic scale all of the way to the continuum. In recent years, much research has been focused on linking models of different length scales, especially from detailed, fully atomistic-to-mesoscopic scales and back.[1] A common way of addressing this issue is to develop coarse-grained (CG) models from full-atomistic simulations by merging groups of chemically connected atoms into superatoms. Potentials between these CG superatoms are derived by averaging over all atomistic degrees of freedom contained in them. The averaged-out detailed degrees of freedom are considered to be unimportant for properties that can be well described on the CG scale. This philosophy of the multiscale simulation enables computer simulations to access the time and length scales characterizing the phenomena of interest, which cannot be reached by brute force atomistic molecular dynamics simulations.

Because it is one of the most common commercial polymers, polystyrene (PS) has a wide application in industry and has attracted considerable attention from researchers in the field of multiscale simulations.[2−11] In the literature, two coarse graining methods are reported for PS.[12,13] One is structure-based iterative Boltzmann inversion (IBI) method[13] which is used in the framework of this article, and the other was developed by Kremer and coworkers[12] by using repulsive Lennard-Jones (LJ)-type potentials for nonbonded interactions between CG superatoms. The similarity between the two methods is to treat the bonded and nonbonded interactions separately. The bonded potentials (bonds, angles, and torsion angles) between CG superatoms in both methods are mean forces obtained directly from the Boltzmann inversion of corresponding distributions extracted from fully atomistic simulations. To understand the physical meaning of these bonded potentials, they can, for example, be mapped onto multipeaked Gaussian functions.[14] For the nonbonded part of CG potentials, in the IBI method,[13] mean forces are used as guessed potentials at the beginning, followed by an iterative modifying procedure according to the difference between radial distribution functions (RDFs) from CG and fully atomistic simulations until the convergence between them are obtained. In Kremer's method,[12] the CG potentials are described by repulsive LJ-type potentials, where the size parameter σ is calculated from the van der Waals radius of superatoms, and the strength of the potential ε is scaled by the temperature.

It seems to be easier to use LJ-type potentials to describe nonbonded interactions than the IBI method, but it is often difficult to reproduce structures precisely on the CG scale used with them, even though different mapping schemes for the same PS melt have been tried.[3,9] (Additionally, they cannot be used in constant-pressure simulations or to model interfaces.) Repulsive LJ-type CG potentials have been applied to study the solvent (ethylbenzene (EB)) diffusion in PS melts,[6] making the assumption that the solvent particles have the same nonbonded potentials and masses as those of the styrene. Such simplifications are not necessary in the IBI method, and any type of structural distribution can be reproduced.[11,15−18] Moreover, the IBI method has been proven to be efficient also for studying dynamic[8,11] as well as rheological[7] properties. For this reason, we prefer to use the IBI method in our study. However, for the IBI potential, a problem arises when its transferability under different thermodynamic conditions is attempted. In a recent paper, the transferability of an IBI potential developed for PS had been checked over a wide range of temperature.[2] It has been found that for the specific mapping scheme,[11] the IBI

* Corresponding author. Tel: +49-6151-16-6537. Fax: +49-6151-16-6526. E-mail: h.qian@theo.chemie.tu-darmstadt.de.
† Technische Universität Darmstadt.
§ University of Manchester.
‡ Polymer Research.

10.1021/ma801910r CCC: $40.75
Published on Web 11/24/2008

Table 1. Atomistic Force Field Potential Energy Function Parameters[a]

	$V(r_{ij}) = 4\varepsilon[(\sigma/r_{ij})^{12} - (\sigma/r_{ij})^6] + q_iq_j/4\pi\varepsilon_0 r_{ij}$		
atoms	ε/kJ·mol^{-1}	σ/nm	q/e
C_{ali}	0.27614 (0.3519)	0.35 (0.3207)	−0.180[b] (0.00)
H_{ali}	0.12552 (0.318)	0.25 (0.2318)	0.060 (0.00)
C_{aro}	0.29288 (0.294)	0.355 (0.355)	−0.115 (−0.115[c])
H_{aro}	0.12552 (0.126)	0.242 (0.242)	+0.115 (+0.115)

	$V_{bonds} = (k_r/2)(r - r_0)^2$	
bonds[d]	r_0/nm	k_r/kJ·mol^{-1}·nm^{-2}
$C_{ali}-C_{ali}$	0.1529	112 131.201
$C_{ali}-H_{ali}$	0.109	142 256.006
$C_{aro}-C_{aro}$	0.140	196 229.602
$C_{aro}-H_{aro}$	0.108	153 552.795
$C_{ali}-C_{aro}$	0.151	132 632.800

	$V(\phi) = (k_\phi/2)(\phi - \phi_0)^2$	
angles	ϕ_0/deg	k_ϕ/kJ·mol^{-1}·rad^{-2}
$H-C_{ali}-H$	107.80 (109.45)	138.072 (306.4)
$C_{ali}-C_{ali}-H$	110.70 (109.45)	156.900 (366.9)
$C_{aro}-C_{ali}-H$	109.5 (109.45)	146.440 (366.9)
$C_{ali}-C_{ali}-C_{aro}$	114.0 (109.45)	263.592 (482.3)
$C_{ali}-C_{aro}-C_{aro}$	120.0 (120.0)	292.880 (376.6)
$C_{aro}-C_{aro}-C_{aro}$	120.0 (120.0)	263.592 (376.6)
$C_{aro}-C_{aro}-H$	120.0 (120.0)	146.440 (418.8)

	$V(\tau) = (k_\tau/2)[1 - \cos 3(\tau - \tau_0)]$	
torsion angles	τ_0/deg	k_τ/kJ·mol^{-1}
$H-C_{ali}-C_{ali}-H$	180.0	1.330512
$H-C_{ali}-C_{ali}-C_{aro}$	180.0	1.933008
$C_{ali}-C_{ali}-C_{ali}-C_{ali}$	(180.0)	(12.0)
$C_{ali}-C_{ali}-C_{ali}-H$	(180.0)	(12.0) (terminal methyl)

	$V(\delta) = (k_\delta/2)(\delta - \delta_0)^2$	
harmonic dihedral angles[e]	δ_0/deg	k_δ/kJ·mol^{-1}·rad^{-2}
$C_{aro}-C_{aro}-C_{aro}-C_{aro}$	0.0	167.4
$C_{aro}-C_{aro}-C_{aro}-H$	0.0	167.4
$C_{aro}-C_{aro}-C_{aro}-C_{ali}$	0.0	167.4

[a] The detailed parameters for the OPLS−AA force field for ethylbenzene and force field parameters (in the parentheses) from ref 24 for the PS chains. The subscripts ali and aro denote aliphatic and aromatic atoms, respectively. [b] The charge on the carbon of CH_2 group of EB is −0.005. [c] The charge on the first carbon atom connected to ethyl group is 0. [d] These OPLS−AA bond parameters are used in both force fields. [e] All atoms that belong to the phenyl ring in PS or EB are kept planar by the use of improper torsion (harmonic dihedral) potentials. Note here: nonbonded interactions are excluded between first and second neighbors, and they are all excluded among all atoms of a given phenyl group.

potential for PS is restricted to a temperature interval of ∼80 K near the optimization temperature where the CG potential is developed. This specificity of the CG potential results in a deviation in thermal expansion behavior from experiment or atomistic simulation. Therefore, it is still a challenge to develop a more temperature-transferable IBI−CG potential for PS.

In this article, we present new CG models for atactic PS and EB, which is essentially the monomer of PS. The newly developed CG potentials are also applied to the mixtures of PS and EB at different concentration and different temperature. For the CG models of the two compounds, the same mapping scheme is used, where one monomer of the PS chain or one EB molecule is represented by one CG bead, which is centered on the center of mass of the corresponding species. We find that the new CG potential for PS is transferable over different temperatures and different chain lengths. In contrast, the CG potential for the EB turns out to be temperature-dependent, and it needs to be modified by a temperature factor when transferred to different temperatures. For the CG models of PS/EB mixtures, the cross interactions between PS and EB are tentatively combined from the CG potentials of PS and EB both arithmetically and geometrically. An optimized geometrical combination rule with constant $x = 0.4$ is proposed, which best fits the densities and RDFs obtained from reference atomistic simulations of two specific mixtures at 400 K. The proposed potentials are also generalized to other CG mixtures of different chain lengths and at different temperatures.

2. Atomistic Molecular Dynamics Simulations

Fully atomistic simulations are carried out by the software package YASP[19] under isothermal−isobaric (NPT) conditions at 1 atm using the Berendsen thermostat (coupling time 0.2 ps) and barostat (coupling time 2.0 ps for PS, and 1.0 ps for EB). The nonbonded interaction cutoff is $r_c = 1.0$ nm with a Verlet neighbor list cut off of 1.1 nm for EB, and 1.1/1.2 nm for PS. We have separately simulated the EB, the melt of PS, and the mixtures of PS and EB. The simulation of EB is carried out at room temperature (298 K) with the all-atom OPLS−AA force field.[20] The system consists of 200 EB molecules. The simulation time is 15 ns. The obtained density of 856 kg/m^3 is in good agreement with experimental value,[21] 862 kg/m^3. The calculated self-diffusion coefficient of EB molecules, 1.35×10^{-5} cm^2/s, is also comparable to the experimental value[22] of 1.99×10^{-5} cm^2/s; the small discrepancy between the values is acceptable for our purpose. For the PS melts, the simulation is carried out at 500 K with 48 chains of 10 monomers in the simulation box. The force field employed for PS has already been used to describe different PS-based materials: PS gels,[23,24] amorphous PS,[25] and crystalline syndiotactic PS.[26] Details of both force fields and parameters are listed in Table 1. Two mixtures of EB and PS are also atomistically simulated. The parameters such

Table 2. Atomistic Systems Simulated in This Study that Act as References for Coarse-Grained Simulations[a]

ethylbenzene content (mol %)	no. of polystyrene chains	no. of ethylbenzene molecules	temp (K)	density (kg/m^3)
100	0	200	298	856
0	48	0	500	944
10	45	57	400	971
25	30	102	400	935

[a] Density values are obtained in NPT simulations. Each polystyrene chain has 10 monomers. The approximate ethylbenzene content in mol % is calculated as the number of ethylbenzene molecules divided by the sum of the number of ethylbenzene molecules and styrene monomers.

as the simulation time step, coupling times for Berendsen thermostat and barostat, and cutoff radius are the same as those in the atomistic simulation of the PS melt. The simulations are carried out at 400 K, which is below the boiling point of EB and above the glass-transition temperature of PS. All atomistically simulated systems of this study are listed in Table 2. They are used as references for the CG simulations below.

A procedure similar to that in ref 6 for setting up the initial configuration was used for the polymeric systems (PS melt and its mixtures with EB) in this study: First, fully stretched (all *trans*-) PS chains were constructed by replicating two different types of monomers that have different absolute configurations; one was *R* and the other was *S*, according to the IUPAC definition. The stereochemistry of the chain was controlled by a uniform random number generator that gave random numbers between 0.0 and 1.0. For each monomer, a random number greater than 0.5 gave the *R* configuration and less than 0.5 gave the *S* configuration. Second, at a very low density value of ~50 kg/m^3, well-separated PS chains (and the added EB molecules in mixtures) were put on a lattice and then equilibrated at 600 K for 1 ns, ensuring their full relaxation of the system without any overlap. Subsequently, the system was compressed under isothermal−isobaric NPT conditions at this temperature for 2 ns until it reached a stable density. Finally, the system was cooled to the desired temperatures, 500 K for pure PS melts and 400 K for PS/EB mixtures with a cooling rate of 0.025 K/ps (200 ps of NVT run, followed by 200 ps of NPT run for each 10 K decrease in temperature). Following this cooling process, a long run of 20 ns was carried out for each system. To check the equilibration of the system, the RDF between carbon atoms (intramolecular correlations in C−C bonds, between C−C−C angles, and between carbons of the phenyl ring are excluded) for the pure PS melts, where equilibration is most difficult and time-consuming, has been calculated. It has an overall excellent agreement with the experimental RDF curve[27] in the whole range of distance with regard to the positions and shapes of the peaks. They are shown in Figure 1. A similar comparison has been made in other simulations.[5,9] The differences in the peak intensities, as discussed in ref 9, can be attributed to the differences in the temperature of the two sets of data: the experimental temperature is much below T_g, whereas the simulations are performed in melt. Because of internal stress in polymer samples below T_g, this temperature difference can indeed lead to small differences in the RDF. However, structural and thermodynamic properties obtained from the simulations, such as density (944 kg/m^3), radius of gyration ($<R_g^2>^{1/2}$ = 0.687 nm), and end-to-end distance ($<R^2>^{1/2}$ = 1.56 nm) at 500 K are in good agreement with the experiment[28] (where a second-order polynomial fit to the equation of state gives a density of 950 kg/m^3) or other simulations[2] ($<R_g^2>^{1/2}$ = 0.646 nm, $<R^2>^{1/2}$ = 1.40 nm).

3. Coarse-Grained Simulations

3.1. Iterative Boltzmann Inversion. The IBI method is used in this study to coarse grain the system. This is a structure-based methodology in which the groups of atoms are merged into superatoms, and the CG potentials between superatoms are derived according to the corresponding structure distributions. The CG potentials of EB and PS are developed at 298 and 500 K, respectively, in this article. A detailed discussion of the IBI method can be found elsewhere.[13] Below we just give a brief description of the essentials.

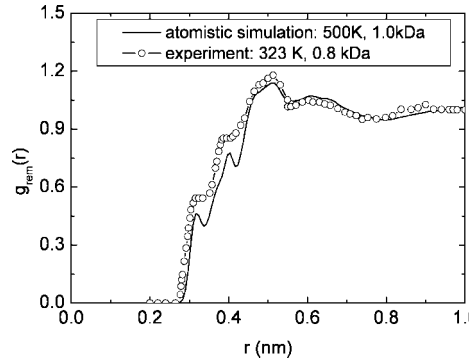

Figure 1. Carbon−carbon radial distribution functions of polystyrene melts obtained from atomistic simulation (—) and wide-angle X-ray diffraction measurements[27] (○). The intramolecular correlations between C−C atoms in bonds, between C−C−C atoms in angles, and between carbons in the phenyl ring are excluded.

In general, the total potential of the system U^{CG} is assumed to be separated into two parts, that is, a bonded (U^{CG}_{bonded}) and a nonbonded ($U^{CG}_{nonbonded}$) part

$$U^{CG} = \sum U^{CG}_{bonded} + \sum U^{CG}_{nonbonded} \quad (1)$$

The stiff bonded potentials in the above equations are approximated by the potentials of mean force of CG degrees of freedom (bond lengths, angles, and dihedral torsions). They are obtained by sampling distribution functions P^{CG} from fully atomistic simulations. In principle, these distributions are functions of bond lengths (r), bond angles (θ), and torsion angles (ϕ), that is, $P^{CG} = P^{CG}(r,\theta,\phi)$. A usual way in the CG simulations is to treat them separately, assuming they are uncorrelated, that is

$$P^{CG} = P^{CG}(r)P^{CG}(\theta)P^{CG}(\varphi) \quad (2)$$

According to this assumption, the independent bonded potentials are given by simple Boltzmann inversion

$$U^{CG}(r) = -k_B T \ln P^{CG}(r) \quad (3)$$

$$U^{CG}(\theta) = -k_B T \ln P^{CG}(\theta) \quad (4)$$

$$U^{CG}(\varphi) = -k_B T \ln P^{CG}(\varphi) \quad (5)$$

Note here that the probability functions in the above expressions are weighted by corresponding metric factors, namely, r^2 for bond length and $1/\sin(\theta)$ for the bending angles.

For the nonbonded interaction between the CG superatoms, the potential of mean force (being a free energy) cannot be used as a potential energy. However, it can be used as a first guess in an iterative refinement

$$U^{CG}_0(r) = -k_B T \ln g^{target}(r) \quad (6)$$

where $g^{target}(r)$ is the target distribution from the reference atomistic simulation. The RDF $g_0^{calculated}(r)$ obtained in the simulation with this trial potential will deviate from the target value. Therefore, we need to modify the potential according to the difference between the calculated and target RDFs. The procedure is iterated in the following way until the two RDFs match

$$U_{i+1}^{CG}(r) = U_i^{CG}(r) + k_B T \ln\left(g_i^{calculated}(r)/g^{target}(r)\right) \quad (7)$$

where $g_i^{calculated}(r)$ is the RDF calculated with the potential $U_i^{CG}(r)$ in the i^{th} iteration.

The merit of this method is in reproducing the structure correlations, not the internal energy. Therefore, the pressure of the system will not be correctly reproduced. To correct the pressure, a linear weak perturbation is added to the potential

$$\Delta U_{lin}(r) = A\left(1 - \frac{r}{r_{cut}}\right) \quad (8)$$

where A is a small constant. Its value is negative or positive depending on whether the pressure is above or below the target value (1 atm). This perturbation vanishes at the cut off of the interaction r_{cut} and $\Delta U_{lin}(0) = A$. This linear modification of the potential and the structure-based iterations of eq 7 are performed concurrently until the target pressure is obtained.

3.2. Mapping. There are four different mapping schemes in the literature[2−4,8−11] for amorphous PS. The first scheme was originally developed in ref 11, where the model consists of chains of superatoms centered on methylene carbons of two different types according to the type of diad (meso or racemo). The mass of a phenyl ring is distributed to the neighboring connecting CG beads. Hence, the CG bead has the same mass as the PS monomer. The second scheme was developed by Sun and Faller,[10] where the model consists of chains of CG beads centered on the methylene backbone carbons carrying the pendant phenyl ring. In this model, each bead represents one PS monomer without distinguishing between different types of beads, different types of bonds, or different types of angles. The last two schemes were developed by Harmandaris and coworkers,[3,9] where one PS monomer is represented by two beads in both mapping schemes. In their first model,[9] the CH_2 group of the backbone chain is represented by one CG bead, whereas the remaining CH group of the monomer in the backbone and its pendant phenyl ring are represented by another CG bead. In their second model,[3] the phenyl ring is represented by one CG bead and another CG bead is the CH_2 of a PS monomer plus the half mass of each one of the two neighboring CH groups along the chain backbone.

As we mentioned in the introduction, our purpose is to find a mapping scheme that is suitable for all of the systems we intend to simulate (liquid EB, melt of PS, and mixture of PS and EB). Considering the single molecule characteristic of EB, we use a mapping scheme similar to that in ref 10. One CG superatom represents one PS monomer; similarly, one CG superatom represents one EB molecule, but they are centered on the corresponding centers of mass instead of on specific carbon atoms, as in previous models. The mapping schemes are plotted in Figure 2. Hence, all CG beads have approximately the same masses, which is important for facilitating long time steps in CG simulations. For the PS chains, two different bead types (*R* and *S*) are defined according to the absolute configuration of the monomer given by the asymmetric −CHR− group defined against the given direction of the carbon backbone. Therefore, there are two different nonbonded interactions, *RR* (or the equivalent *SS*) and *RS* (or *SR*); two types of bonds, *R*−*R* (or *S*−*S*) and *R*−*S* (or *S*−*R*); three types of angles, *R*−*R*−*R* (or *S*−*S*−*S*), *R*−*R*−*S* (or *S*−*S*−*R*, *R*−*S*−*S*, *S*−*R*−*R*), and *R*−*S*−*R* (or *S*−*R*−*S*); and ten different types of torsions for defining the stereochemistry of the chains. Consequently, we define two different potentials for the bond interactions and three for the angle interactions, but we use only one for the nonbonded interaction and one for the torsions, which are averaged over all of the possibilities. The use of only one type of torsion and nonbonded interaction is based on the fact that the chemical details of the monomer are the same irrespective of their absolute configurations defined by the asymmetric −CHR− groups. This is also proven by the resulting different nonbonded RDFs between *RR* (or *SS*) and *RS* (or *SR*) pairs from CG simulations, which match the target RDFs from atomistic simulations very well, as will be shown below. The tacticity of the chains in the CG model is captured by the definition of two different bonds and three different angles. In the CG simulation of PS melts, the nonbonded interactions between first and second neighbors along the chain are excluded. The interactions between the third neighbors are included in this model because otherwise unreasonable overlaps between CG beads will happen.

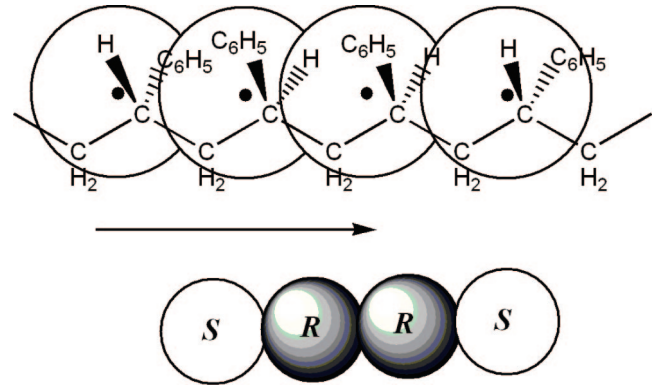

Figure 2. Illustration of the coarse graining mapping schemes for (a) ethylbenzene and (b) polystyrene. One coarse-grained bead corresponds to one ethylbenzene molecule or one polystyrene monomer (−(C_6H_5)C_2H_3−). The centers of the beads are indicated by filled circles on the real center of mass of the corresponding atomistic chemical structure. Bead types *R* and *S* are defined for the polystyrene beads according to the absolute configuration of the monomer given by the asymmetric −CHR− group, which is defined against the given direction of the carbon backbone indicated by the arrow.

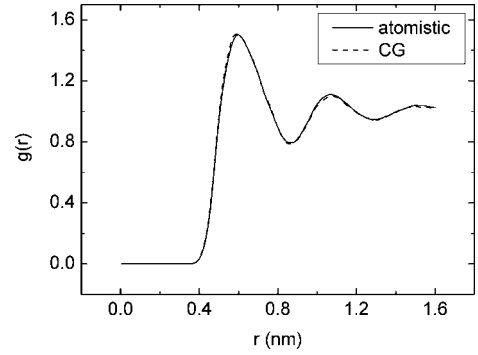

Figure 3. Calculated radial distribution functions between the center of mass of ethylbenzene molecules in both the atomistic (—) and coarse-grained (CG) (---) models at room temperature 298 K.

3.3. Details of Coarse-Grained Simulations. All CG simulations in this work were carried out by the use of the IBISCO code,[29] which is able to handle numerical tabulated potentials. The Berendsen thermostat (coupling time 0.5 ps) and barostat (coupling time 5 ps with an isothermal compressibility of 1.0×10^{-6} kPa^{-1})were used. The nonbonded interactions were truncated beyond 1.6 nm with a neighbor list cut off of 1.7 nm. The simulations of EB and PS systems were carried out at 298 and 500 K, respectively, as in the atomistic simulations. In the case of EB, the time step is set up to 10 fs, whereas it is 5 fs for the PS melts. We simulate 200 EB molecules and 48 PS chains of length 10, respectively.

3.4. Development of Coarse-Grained Potentials. In Figure 3, the good matching between the reference nonbonded RDF from the atomistic simulation and that from the CG simulation after the IBI procedure is shown for the EB model. The duration

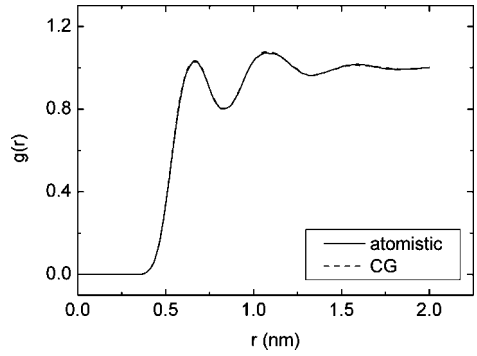

Figure 4. Calculated nonbonded radial distribution functions of the centers of mass of monomers from atomistic (—) and coarse-grained (CG) (---) simulations of atactic polystyrene at 500 K.

of the CG simulation for extracting the RDF was 20 ns under NPT conditions. The final IBI potential of EB gave a density value of 852 kg/m^3, which is consistent with atomistic simulation and experiment (cf. Section 2).

For the PS model, the IBI procedure achieved a good match for both nonbonded and bonded distributions between centers of mass of PS monomers. (See Figures 4 and 5, respectively.) Although the same nonbonded interaction potential was used for *RR* (or *SS*) and *RS* (or *SR*) in the CG model, we find in Figure 6 that their corresponding distributions from atomistic simulations are well reproduced. The final optimized potential for PS gives a density of 937 kg/m^3, a gyration radius of 0.678 nm, and an end-to-end distance of 1.67 nm in NPT simulations. All of these results are in good agreement with the corresponding atomistic results reported in Section 2. Although, in this work, we are not interested in investigating dynamical properties, it is good practice to check whether unphysical bond crossing among the polymer chains is avoided in our CG simulation. The RDF of bond centers (excluding centers of neighboring bonds) plotted in Figure 7 indicates that no bond crossing happens in the simulation.

3.5. Coarse-Grained Simulations of Longer Polystyrene Chains. To check the performance of the CG PS potential further, we constructed PS systems of different chain lengths ranging from 30 to 120 monomers. The preparation of the CG simulation boxes of PS of different chain lengths was done in the following way: At the beginning, the bond length was fixed at the most populated point. In this study, it was ~0.5 nm (Figure 5a,b). Then, all chains were generated by means of a continuous random walk in the box without taking into account the distribution of angles and torsions. The initial density was low (650 kg/m^3). The initially generated CG PS configurations had strong overlaps between atoms. To remove them, the systems were first equilibrated for 50 ps under NVT conditions with a reduced time step of 0.5 fs using the bond interaction and soft-core nonbonded interactions. The short-range part ($<$0.2 nm) of the nonbonded potential was replaced by a plateau ($V = 1.5 \times 10^{-17}$ J) in the soft-core potential. The nonbonded interactions were reintroduced to the system after the initial 50 ps relaxation without the angle and torsion potentials. During the following NVT equilibrations, the angle potentials were added first, followed by 1 ns relaxation, and then the torsion potentials were introduced, followed by another 1 ns. The time step was slowly increased during the whole process, from $dt =$ 0.5 fs in the first equilibration run with bonds, 2 fs with angles, to the final value 5 fs with torsions. Finally, the system equilibrated at low density under NVT conditions was compressed in isothermal−isobaric NPT runs with full interactions for 10 ns, which was more than enough to reach the equilibrium density. A production run of 20 ns was carried out after the equilibration for each system. The dimensions of the chains (radius of gyration and end-to-end distance) as a function of the chain length are presented in Figure 8 on log−log scales. The chain length is varied from $N = 10$ to 120. The chain dimensions show good agreement with other studies on PS.[2,8] Linear fits in both Figures give scaling exponents of $\nu = 0.581$ and 0.589, respectively, which is the value of excluded volume chains because the chains are short in this study. A previous CG simulation of atactic PS[4] indicated that the Flory exponent of 0.5 is reached for chains of $N \approx 300$ and beyond.

4. Temperature Transferability of the Coarse-Grained Force Fields

To address the issue of the temperature transferability of CG potentials, simulations at different temperatures for both CG and atomistic models were carried out. For the single-molecule EB model, the simulations at different temperature were carried out from the same initial configurations. For the atomistic polymeric PS melts, to avoid being trapped in local minimum, the systems were continuously cooled from 500 K under constant pressure with a cooling rate of 0.2 K/ps. The temperature was decreased in steps of 10 K. For every temperature step of 10 K, the simulation time was 100 ps under NVT conditions, followed by 400 ps under NPT conditions. In the CG PS simulations, because of the faster computation, simulation runs for every 10 K step were 2.5 ns (NVT), followed by 10 ns (NPT). In the following paragraphs, the details of the temperature transferability are discussed for both models.

4.1. Ethylbenzene Model. For the EB model, the CG potential was developed at room temperature 298 K, and it was tested from 238 to 380 K. The thermal expansion behavior is plotted in Figure 9. The solid circles are from atomistic simulations and are used as a target reference. The thermal expansion coefficient ($\alpha = V^{-1}(\partial V/\partial T)$) calculated from this line is $\alpha = 1.3 \times 10^{-3}$ K^{-1} and is consistent with the experimental value ($\alpha = 1.02 \times 10^{-3}$ K^{-1}).[21] When the CG potential developed at 298 K was directly transferred to other temperatures, the resulting thermal expansion (□ in Figure 9) had a big deviation from the atomistic simulation. This means that for the case of EB the CG potential is temperature-dependent. The RDFs calculated from atomistic MD simulations at different temperature (238, 298, and 380 K) are shown in Figure 10, and they show the expected differences.

Considering the relationship between the potential and the RDF, $g(r,T) \approx \exp(-u(r,T)/kT)$, where k is Boltzmann's constant, the temperature dependence of CG potential is not surprising. Different RDFs $g(r,T)$ correspond to different potentials $u(r,T)$. To find out this T dependence of the potential $f(T)$, we suppose that the T dependence and r dependence of the potential can be separated from each other, $u(r,T) = u(r)f(T)$. Trial simulations were carried out with potentials modified by a linear temperature scaling factor of $f(T) = T/T_0$, where at $T_0 = 298$ K, the CG potential had been developed. Interestingly, we found that the density of the system was constant at different temperatures ($\alpha = 0$), as shown by ■ in Figure 9. Even the RDFs at 238, 298, and 380 K coincided to almost within line thickness (Figure 11). In Figure 9, the target density is located between curves calculated from the unmodified CG potential and the CG potential multiplied by T/T_0. This finding lead us to try a temperature scaling factor of $f(T) = \sqrt{T/T_0}$. The resulting thermal expansion behavior (△ in Figure 9) matched the atomistic behavior well. With this modification of the CG potential, the RDFs were calculated at two different temperatures, again 380 and 238 K, where one was much higher than 298 K and the other was much lower. Again, they matched the atomistic curves calculated at the same temperatures (Figure

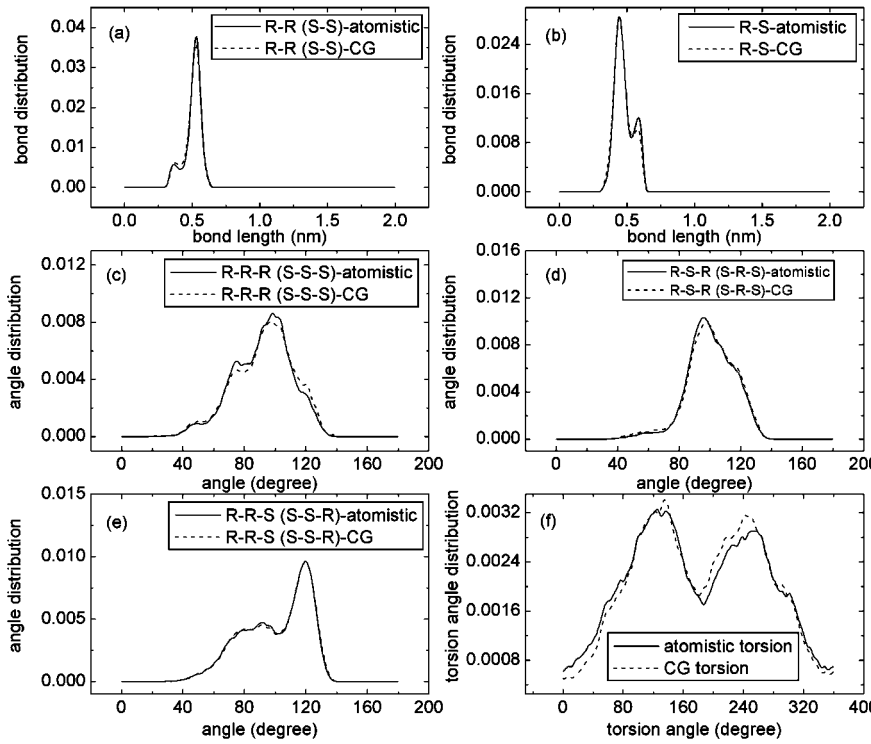

Figure 5. Calculated bonded distributions between centers of mass of monomers from atomistic (—) and coarse-grained (CG) (---) simulations of atactic polystyrene at 500 K. (a) Bond length distribution for $R-R$, (b) bond length distribution for $R-S$, (c) angle distribution for $R-R-R$, (d) angle distribution for $R-S-R$, (e) angle distribution for $R-R-S$, and (f) torsion distribution averaged over all combinations of R and S.

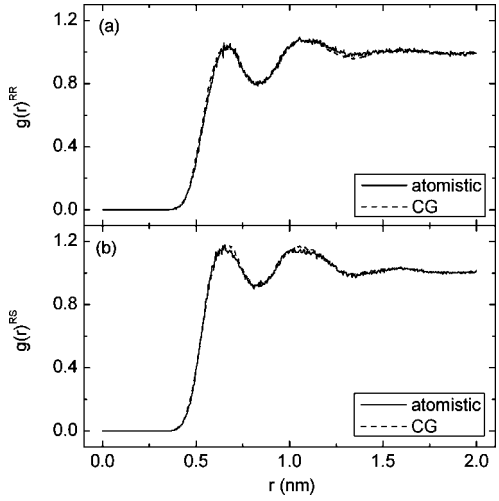

Figure 6. Calculated nonbonded radial distribution functions from atomistic (—) and coarse-grained (CG) (---) simulations of atactic polystyrene at 500 K (a) between R and R monomers (or the equivalent SS) and (b) between R and S monomers.

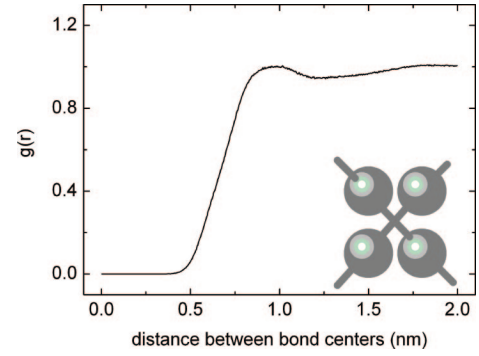

Figure 7. Calculated radial distribution functions between un-neighboring bond centers in coarse-grained (CG) polystyrene melts at 500 K. The inset shows the scenario in which two bonds cross each other, where two bond centers have a distance of close to 0. The maximum bond length is 0.64 nm.

12a,b) very well. They justify the temperature factor of $\sqrt{T/T_0}$ for CG potential.

This temperature dependence of the potential can be tentatively rationalized by the relationship between the RDF and the potential, $g(r,T) \approx \exp(-u(r,T)/kT)$. When the potential is assumed to have the form of $u(r,T) = u(r)f(T)$, as discussed above, the RDF can be factorized as

$$g(r,T) \approx \exp(-[u(r)f(T)]/kT) \approx \exp\left(-\frac{u(r)}{kT_0}F(T)\right) \qquad (9)$$

where $F(T) = f(T)(T_0/T)$; $T_0 = 298$ K is the temperature where we develop the CG potential, and $g(r,T_0)$ is the RDF at 298 K.

This exponential relationship between RDFs of different temperatures can help us to understand the results and the relationship $u(r,T) = u(r,T_0)\sqrt{T/T_0}$. When we modify the CG potential with the linear relationship $f(T) = T/T_0$, the exponent in the above equation is $F(T) = f(T)(T_0/T) = 1$. Hence, $g(r,T) = g(r,T_0)$, which is the result in Figure 10. For the temperature factor $f(T) = \sqrt{T/T_0}$, the exponent becomes $F(T) = f(T)(T_0/T) = \sqrt{T/T_0}$, and hence

$$g(r,T) = g(r,T_0)\sqrt{\frac{T_0}{T}} \qquad (10)$$

If we extrapolate the RDFs at $T = 238$ and 380 K from that at $T_0 = 298$ K in atomistic simulations by using this relation, then we can find that the extrapolated RDFs perfectly coincide with the RDFs obtained from atomistic simulations at corresponding temperatures (Figure 13). The coincidence in this Figure is further proof for the temperature dependence of the CG potential, $u(r,T) = u(r)\sqrt{T/T_0}$.

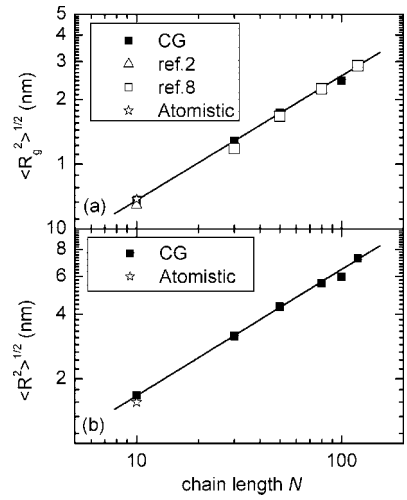

Figure 8. Calculated values (■) of (a) radius of gyration and (b) end-to-end distance as a function of the chain length N of the polystyrene chains in coarse-grained (CG) simulations. Their values for a chain length of $N = 10$ are compared with those of atomistic models (☆). The gyration radii are compared with other simulation studies (△ and □ in a from refs 2 and 8, respectively).

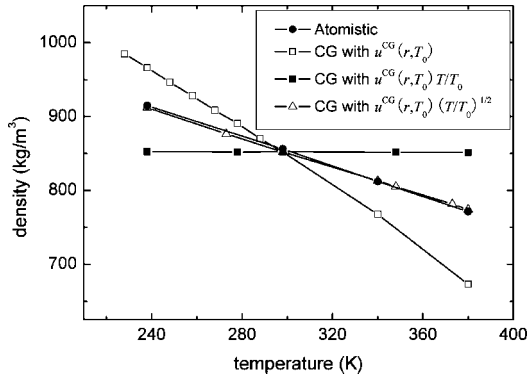

Figure 9. Thermal expansion of the ethylbenzene system obtained in atomistic and coarse-grained (CG) simulations. The results from CG simulations with unmodified potentials that are developed at 298 K (□) have an obvious deviation from the atomistic model (●). This deviation vanishes when the CG potential is scaled by a temperature factor of $\sqrt{T/T_0}$ (△). The system has the same thermal expansion behavior as that in the atomistic model. The CG simulations with the potentials modified by the linear factor of T/T_0 resulted in the same densities at different temperatures (■). The CG force field has been optimized at the temperature $T_0 = 298$ K.

4.2. Polystyrene Model. For the PS model, the CG potential was developed at 500 K. It was tested down to 400 K as the system was cooled. The thermal expansion behavior of the PS model is reported in Figure 14. The results are compared with atomistic simulations, which give a thermal expansion coefficient $\alpha = 5.4 \times 10^{-4}$ K^{-1},which is the same as that in the experiment,[30] $\alpha = 5.5 \times 10^{-4}$ K^{-1}. Densities were normalized (divided) by the values at 500 K. In the atomistic simulations, we found that the nonbonded RDF as well as the bonded distributions of the system did not change with the temperature (Figure 15). This indicates that the CG potential of PS might be temperature-independent, which is indeed found by the density curves in Figure 14. The atomistic curve is well reproduced by CG simulations with the CG potential developed at 500 K. The same CG potential was used at all temperatures without any modification. The nonbonded and bonded distributions at other temperatures were also in good agreement with the atomistic models.

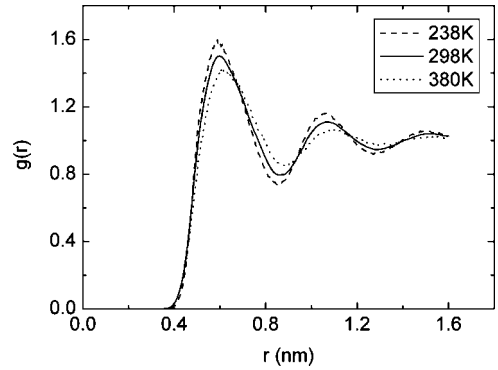

Figure 10. Atomistic radial distribution functions between the centers of mass of ethylbenzene molecules calculated at different temperatures. One is at 238 K (---) (much lower than room temperature (298 K)), and the other is at 380 K (•••) (much higher than room temperature). They are plotted together with the RDF of 298 K (—) from Figure 2.

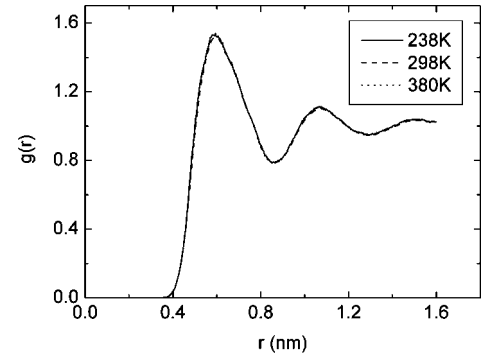

Figure 11. Radial distribution functions between the centers of mass of ethylbenzene molecules calculated for the coarse-grained (CG) model at different temperatures with the CG potential developed at $T_0 = 298$ K being multiplied by a linear temperature scaling factor T/T_0.

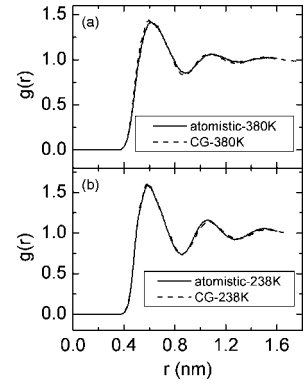

Figure 12. Radial distribution functions between centers of mass of ethylbenzene molecules from atomistic (—) and coarse-grained (CG) (---) simulations at two different temperatures: (a) 380 and (b) 238 K. The CG model developed at $T_0 = 298$ K was multiplied with a temperature scaling factor $\sqrt{T/T_0}$.

One question arises: Why is the current model temperature-independent, whereas the previous CG models[2,11] of PS were temperature-dependent? The temperature transferability was allowed down to only 430 K in the previous CG models,[2] below which a deviation of the thermal expansion coefficient from the atomistic model resulted. One possible reason is that an explicit torsion angle potential was used in our model but not in the previous models.[2,11] To clarify the influence of the torsion potential on the transferability, we developed the CG potential again with the same mapping but with the torsion potential

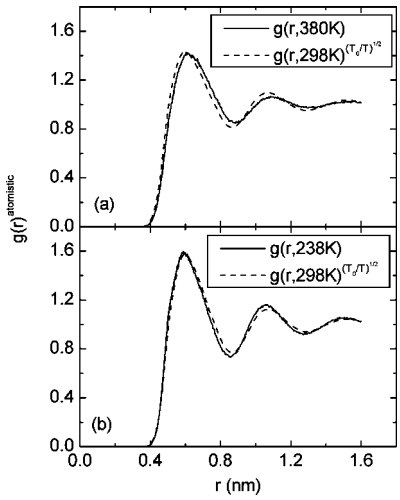

Figure 13. Radial distribution functions (RDFs) between centers of mass of ethylbenzene (EB) molecules at (a) 380 and (b) 238 K. The solid curves are directly calculated by atomistic simulations at the respective temperatures. The dashed curves are extrapolated from the atomistic RDF at $T_0 = 298$ K using eq 10.

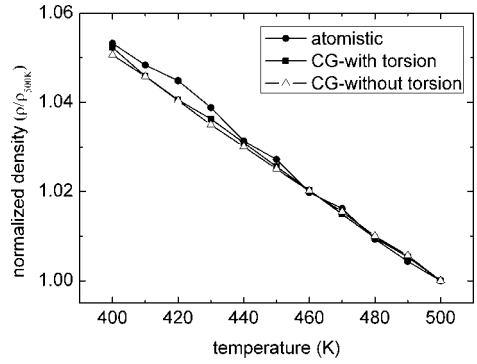

Figure 14. Thermal expansion behavior of the polystyrene decamer melts obtained from atomistic (●) and from coarse-grained (CG) simulations with torsion potential included (■) or excluded (△). The densities are normalized (divided) by the values at 500 K.

removed. This torsion-excluded CG potential was also temperature-transferable and resulted in the same thermal expansion behavior (△ in Figure 14). This result indicates that the temperature transferability of the CG potential does not depend on the presence of a torsion potential. A possible reason for the deviation in the thermal expansion behavior of the previous CG models from atomistic simulations is the mapping scheme and the location of the CG bead center. The superatom location is the most significant qualitative difference between the schemes. This is supported by a recently developed CG model for a chainlike ionic liquid,[31] which successfully described the density over a wide temperature range without any temperature correction. Here the CG bead center was put on the real center of mass, and the thermal expansion of the atomistic simulation was well reproduced by the CG model. At the moment, it is not clear for which other polymer systems and under which conditions a CG potential is temperature-independent. Investigations of more polymer systems are needed and will be carried out in the future. The temperature transferability of the CG PS potential is expected at least in the temperature range that is studied in this article, that is, 400−500 K.

5. Combination Rules for Coarse-Grained Interactions between Styrene Units and Ethylbenzene

In the CG simulation of mixtures of PS and EB, we have the interactions between styrene pairs (PS−PS) and ethylbenzene pairs (EB−EB) of Section 4. In addition, there is the cross interaction between styrene units and ethylbenzene molecules (PS−EB). Rather than always having to parametrize the interactions between unlike pairs from atomistic simulations of mixtures, we would like to estimate them from the known potentials for neat systems. In atomistic simulations, one uses combination rules like the Lorentz−Berthelot mixing rules for LJ parameters. Here we follow an analogous route and try two different combination rules for obtaining the cross PS−EB interaction. One is arithmetic (eq 11) and the other is geometric (eq 12).

$$u_{\mathrm{PS-EB}} = x u_{\mathrm{EB-EB}} \sqrt{T/T_0} + (1-x) u_{\mathrm{PS-PS}} \tag{11}$$

$$u_{\mathrm{PS-EB}} = \left(u_{\mathrm{EB-EB}} \sqrt{T/T_0} + C\right)^x (u_{\mathrm{PS-PS}} + C)^{1-x} - C \tag{12}$$

The x is a constant between 0 and 1. It is manually varied from 0.1 to 0.9 for both combination rules in steps of 0.1; $u_{\mathrm{EB-EB}}$, $u_{\mathrm{PS-PS}}$, and $u_{\mathrm{PS-EB}}$ are CG potentials between EB−EB, PS−PS, and PS−EB, respectively. In the geometrical combination rule, the EB−EB and PS−PS potentials are shifted up by a small positive constant C before combination. The combined potential is shifted back to zero at the cutoff distance after combination. From the simulations, the most appropriate combination rule and constant x are selected on the basis of the reproduction of the density and the structure distributions from reference atomistic systems. For computational efficiency, torsion interactions are excluded here. The inherent temperature dependence of the CG potential between EB−EB molecules is still accounted for by the temperature factor of $\sqrt{T/T_0}$.

The two PS/EB mixtures (cf. Table 2) with 10 mol % and 25 mol % of EB are simulated. All densities obtained using the two combination rules with various values of x are listed in Table 3 together with the percentage deviations from target reference values of the atomistic simulations. The results show that the geometric rule, eq 12 with $x = 0.4$ as the best choice, gives densities of 966 kg/m^3 and 939 kg/m^3 for the two mixtures, respectively. The deviations of the CG density from atomistic simulations are ∼0.5% for both systems. Actually, the arithmetic combination rule with $x = 0.4$ is choice, which also gives good results (Table 3). After the correct density values were obtained, the different structure distributions were calculated and compared with those from atomistic simulations. Good agreement was found for the systems with the geometric rule (eq.12) and $x = 0.4$. As an example, we show the results of the second mixture with 25 mol % EB: The nonbonded RDFs between EB−EB molecules, between EB−PS pairs, and between PS−PS monomers are plotted in Figure 16. The bond length and angle distributions in the PS chain are also shown in Figures 17 and 18, respectively. Good agreement between CG and atomistic simulations is observed in these Figures.

This potential is also applied to a PS/EB mixture with a longer PS chain length of 96 monomers at 463 K, which has 10 mol % of EB. The density obtained in our CG simulation is 988 kg/m^3. We have not calculated the density using our atomistic model from which the CG models were derived. However, the united atom model of ref 6 gives a close density value of 975 kg/m^3. The intermolecular RDFs between EB−EB molecules, between EB−PS, and between PS−PS monomers in the CG simulation are calculated and plotted in Figure 19 together with the corresponding RDFs from this united-atom model.[6] They agree well with each other. The residual difference in the PS−PS RDF (Figure 19c) comes from the two different atomistic models; in our work, the full atomistic model is used instead of the united-atom model in ref 6.

In addition, the proposed geometric combination rule (eq 12 with $x = 0.4$) is generalized to different temperatures. When it is applied to the thermal expansion behavior of the mixture with

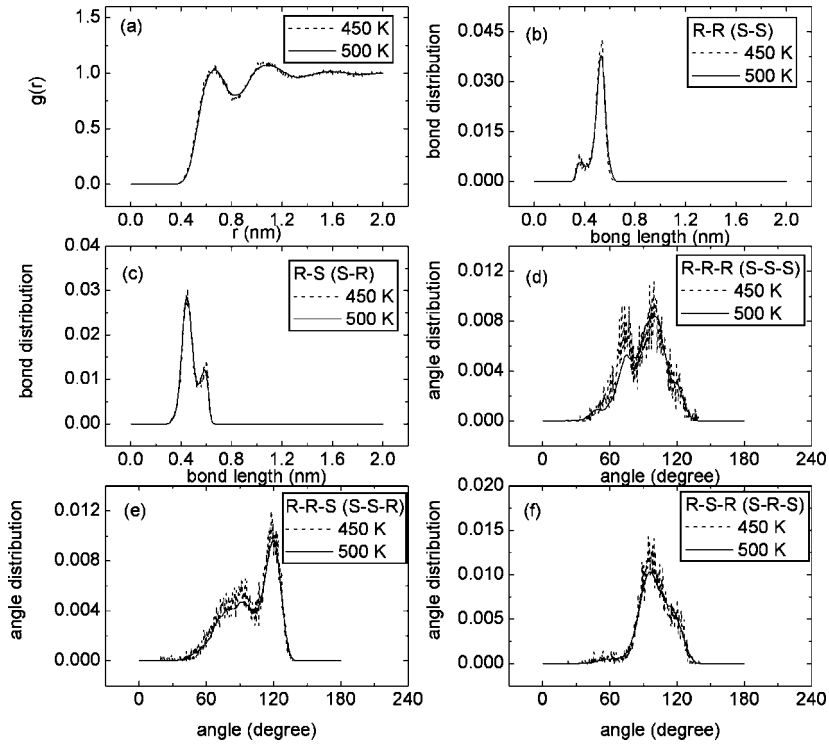

Figure 15. Calculated nonbonded radial distribution functions (RDF) and bonded distributions between centers of mass of polystyrene monomers from atomistic simulation at two different temperatures, 450 (---) and 500 K (—). (a) Nonbonded RDF, (b) bond length distribution for $R-R$, (c) bond length distribution for $R-S$, (d) angle distribution for $R-R-R$, (e) angle distribution for $R-R-S$, and (f) angle distribution for $R-S-R$.

Table 3. Density (kg/m^3) from CG Simulations and its Percentage of Deviations (%) from the Reference Atomistic Results of Table 2[a]

	10 mol % ethylbenzene		25 mol % ethylbenzene	
combination constant x	density (kg/m^3)	deviation (%)	density (kg/m^3)	deviation (%)
0.1	947 (948)	−2.47 (−2.37)	915 (916)	−2.14 (−2.03)
0.2	951 (954)	−2.06 (−1.75)	917 (921)	−1.93 (−1.50)
0.3	956 (960)	−1.54 (−1.13)	923 (928)	−1.28 (−0.75)
0.4	962 (966)	−0.93 (−0.52)	932 (939)	−0.32 (0.43)
0.5	968 (973)	−0.31 (0.21)	944 (952)	0.96 (1.82)
0.6	975 (980)	0.41 (0.93)	957 (965)	2.35 (3.21)
0.7	982 (986)	1.13 (1.54)	972 (980)	3.96 (4.81)
0.8	990 (994)	1.96 (2.37)	988 (995)	5.67 (6.42)
0.9	998 (1000)	2.78 (2.99)	1006 (1009)	7.59 (7.91)

[a] Cross-interaction potentials between styrene and ethylbenzene u_{PS-EB} are combined arithmetically or geometrically (in parentheses) by the use of eqs 11 and 12, respectively. The combination constant x varies from 0.1 to 0.9. The temperature is 400 K.

an EB content of 25 mol % (Table 2), the CG simulation gives the exact same thermal coefficient as that of the atomistic simulations (Figure 20) in the temperature range between 360 and 410 K, which is between the glass-transition temperature of PS and the boiling point of EB. The density gap between two lines is constant around 0.5% over the whole temperature range.

6. Conclusions

In this article, we have developed CG models for liquid EB and for PS melts by using the structure-based and pressure-corrected IBI method. The EB model is developed at room temperature; one CG superatom represents one EB molecule. The density of the system and the RDF between centers of mass of EB molecules extracted from the full atomistic model are exactly reproduced in this CG model.

The PS model is developed at 500 K. A similar mapping scheme as that for the EB model is adopted. Atoms in each PS monomer are merged into one CG superatom located at the center of mass of the repeat unit. The CG superatoms are distinguished as R and S according to their absolute configuration of the parent monomers (R or S). In consequence, two different types of bonds and three different angles are defined to capture the stereochemistry of the chains. For the nonbonded potentials, only one potential is developed, which averages the two

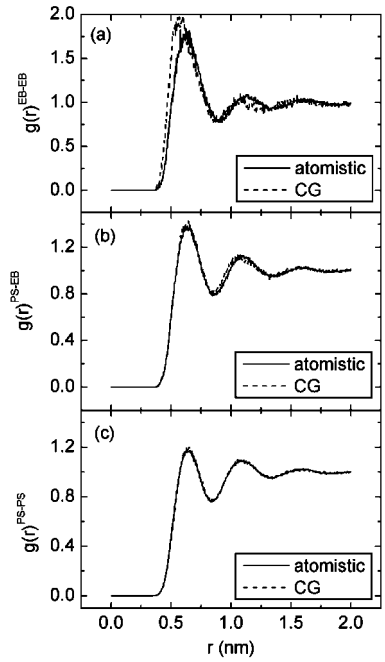

Figure 16. Center of mass radial distribution functions from atomistic (—) and coarse-grained (CG) (---) simulations of a polystyrene/ethylbenzene (PS/EB) mixture at 400 K: (a) EB−EB; (b) PS−EB, and (c) PS−PS. The content of EB is 25 mol %; PS consists of decamers. The interactions between PS and EB beads are combined from eq 12 with $x = 0.4$.

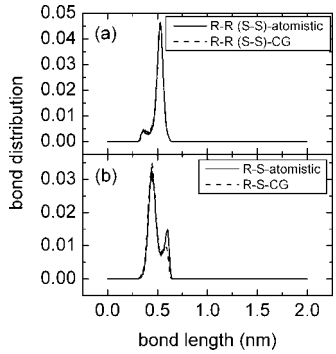

Figure 17. Bond length distributions in polystyrene chains from atomistic (—) and coarse-grained (CG) (---) simulations of the polystyrene/ethylbenzene (PS/EB) mixtures at 400 K for bonds (a) *R*−*R* and (b) *R*−*S*. The content of EB is 25 mol %; the PS chains are 10 monomers long.

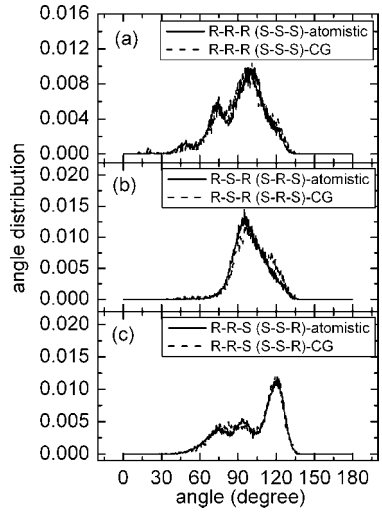

Figure 18. Angle distributions in polystyrene chains calculated from atomistic (—) and coarse-grained (CG) (---) simulations of the polystyrene/ethylbenzene (PS/EB) mixtures at 400 K. The content of EB is 25 mol %; the PS chains are 10 monomers long. (a) Angle *R*−*R*−*R*, (b) angle *R*−*S*−*R*, and (c) angle *R*−*R*−*S*.

possibilities of *RR* (*SS*) and *RS* (*SR*). Nonetheless, the resulting nonbonded distributions between the different species are still in good agreement with atomistic simulations. Other properties, such as the density of the system, the radius of gyration, and the end-to-end distance of PS chains of different length are also in good agreement with the atomistic reference simulations or with other studies.

Both CG models, EB and PS, which are developed and optimized at a single thermodynamic state (temperature T_0 and ambient pressure), are transferred to and tested at a broad range of temperature. Both CG potentials are temperature-transferable, but a temperature scaling factor of $\sqrt{T/T_0}$ is needed for the EB potential. All CG simulations at different temperatures in this study for both EB and PS systems give the correct thermal expansion behaviors. At the same time, the structure distributions in the corresponding atomistic models are well reproduced. As to why the CG potential for the molecular liquid EB needs a temperature correction whereas that for the polymer PS can be used unchanged over a range of 100 K, we have no definitive answer. One may speculate that the nonbonded interactions dominate the density−temperature relation for the molecular liquid, whereas the polymer density is much more controlled by the bonds linking the repeat units. The nonbonded interactions are soft and susceptible to a change in temperature; the chemical bonds are stiff. Thus, whereas it is possible that the

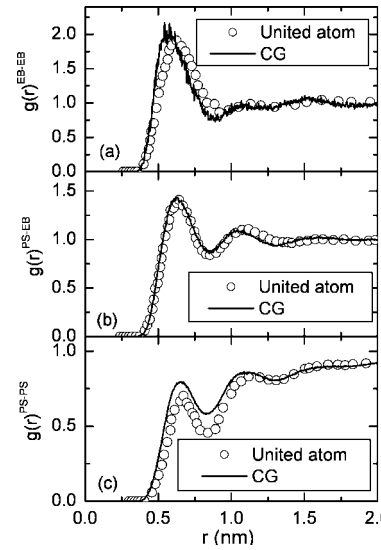

Figure 19. Intermolecular radial distribution functions (RDF) between centers of mass of styrene (PS) monomers, ethylbenzene (EB) molecules, or both obtained from coarse-grained (CG) simulations (—) compared with the united-atom model (○) of ref 6 for a mixture of PS (96-mers) and EB (10 mol %) at $T = 463$ K. RDF between (a) EB−EB, (b) PS−EB, and (c) PS−PS.

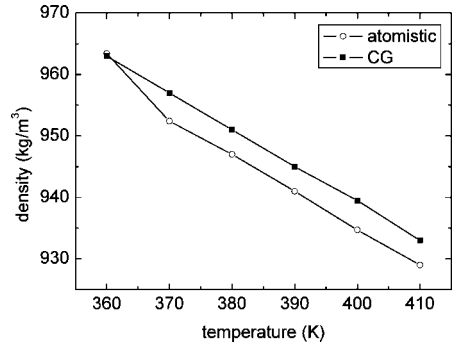

Figure 20. Thermal expansion behavior obtained from atomistic (○) and coarse-grained (■) simulations for a specific polystyrene/ethylbenzene mixture. The content of EB is 25 mol %; the PS chains are 10 monomers long.

polymer, in principle, also needs some massaging of its CG nonbonded interactions as the temperature changes, this need might be masked by the temperature-insensitive bonded interactions.

Apparently, the temperature scaling factor is suitable for only simple fluids. This observation is, however, based on only the one example of a single bead model of EB. It is not clear, at the moment, whether it is suitable for other fluids. Investigations of more liquids and polymer systems will be carried out in the future. In this context, it may be interesting that there exists a coarse-graining scheme for one other molecular fluid, supercritical CO_2, which has been described by LJ plus quadrupole−quadrupole interactions and has been simulated by Monte Carlo. This model accurately captures the thermophysical properties.[32]

For mixtures of EB and PS, an empirical mixing rule was finally found and optimized for the cross interactions: $u_{PS-EB} = (u_{EB-EB}\sqrt{T/T_0} + C)^x(u_{PS-PS} + C)^{1-x} - C$ with $x = 0.4$. The potentials estimated using this combination rule are tested for two mixtures of different contents of EB at 400 K where the PS molecules are 10 monomers long. The densities and structure distributions obtained by CG simulations are in good agreement with corresponding atomistic results. Another CG system with 10% EB and longer PS chains of 96 monomers is also constructed in this study,

but at a different temperature of 463 K. The reference density value of 975 kg/m^3 as well as the structure correlations from atomistic simulations[6] are well reproduced. The new combination rule for the PS−EB cross also reproduces the density as a function of temperature for the mixtures.

Acknowledgment. We are grateful for financial support from BASF SE, Ludwigshafen. We thank HHLR supercomputer centre at the Technische Universität Darmstadt for providing computing resources.

References and Notes

(1) Müller-Plathe, F. *ChemPhysChem* **2002**, *3*, 754.
(2) Carbone, P.; Varzaneh, H. A. K.; Chen, X.; Müller-Plathe, F. *J. Chem. Phys.* **2008**, *128*, 064904.
(3) Harmandaris, V. A.; Reith, D.; van der Vegt, N. F. A.; Kremer, K. *Macromol. Chem. Phys.* **2007**, *208*, 2109.
(4) Spyriouni, T.; Tzoumanekas, C.; Theodorou, D.; Müller-Plathe, F.; Milano, G. *Macromolecules* **2007**, *40*, 3876.
(5) Santangelo, G.; di Matteo, A.; Müller-Plathe, F.; Milano, G. *J. Phys. Chem. B* **2007**, *111*, 2765.
(6) Harmandaris, V. A.; Adhikari, N. P.; van der Vegt, N. F. A.; Kremer, K.; Mann, B. A.; Voelkel, R.; Weiss, H.; Liew, C. C. *Macromolecules* **2007**, *40*, 7026.
(7) Chen, X.; Carbone, P.; Cavalcanti, W. L.; Milano, G.; Müller-Plathe, F. *Macromolecules* **2007**, *40*, 8087.
(8) Sun, Q.; Faller, R. *Macromolecules* **2006**, *39*, 812.
(9) Harmandaris, V. A.; Adhikari, N. P.; van der Vegt, N. F. A.; Kremer, K. *Macromolecules* **2006**, *39*, 6708.
(10) Sun, Q.; Faller, R. *Comput. Chem. Eng.* **2005**, *29*, 2380.
(11) Milano, G.; Müller-Plathe, F. *J. Phys. Chem. B* **2005**, *109*, 18609.
(12) Tschöp, W.; Kremer, K.; Batoulis, J.; Bürger, T.; Hahn, O. *Acta Polym.* **1998**, *49*, 61.
(13) Reith, D.; Pütz, M.; Müller-Plathe, F. *J. Comput. Chem.* **2003**, *24*, 1624.
(14) Milano, G.; Goudeau, S.; Müller-Plathe, F. *J. Polym. Sci., Part B: Polym. Phys.* **2005**, *43*, 871.
(15) Carbone, P.; Negri, F.; Müller-Plathe, F. *Macromolecules* **2007**, *40*, 7044.
(16) Li, X.; Kou, D.; Rao, S.; Liang, H. *J. Chem. Phys.* **2006**, *124*, 204909.
(17) Ashbaugh, H. S.; Patel, H. A.; Kumar, S. K.; Garde, S. *J. Chem. Phys.* **2005**, *122*, 104908.
(18) Chen, L.-J.; Qian, H.-J.; Lu, Z.-Y.; Li, Z.-S.; Sun, C.-C. *J. Phys. Chem. B* **2006**, *110*, 24093.
(19) Müller-Plathe, F. *Comput. Phys. Commun.* **1993**, *78*, 77.
(20) Jorgensen, W. L.; Maxwell, D. S.; Tirado-Rives, J. *J. Am. Chem. Soc.* **1996**, *118*, 11225.
(21) Matilla, A. D.; Aicart, E.; Diaz Pena, M.; Tardajos, G. *J. Solution Chem.* **1989**, *18*, 143.
(22) Zgadzai, O. E.; Maklakov, A. I. *Acta Polym.* **1985**, *36*, 621.
(23) Witt, R.; Sturz, L.; Dölle, A.; Müller-Plathe, F. *J. Phys. Chem. A* **2000**, *104*, 5716.
(24) Müller-Plathe, F. *Macromolecules* **1996**, *29*, 4782.
(25) Schmitz, H.; Müller-Plathe, F. *J. Chem. Phys.* **2000**, *112*, 1040.
(26) Milano, G.; Guerra, G.; Müller-Plathe, F. *Chem. Mater.* **2002**, *14*, 2977.
(27) Londono, J. D.; Habenschuss, A.; Curro, J. G.; Rajasekaran, J. J. *J. Polym. Sci., Part B: Polym. Phys.* **1996**, *34*, 3055.
(28) Hocker, H.; Blake, G. J.; Flory, P. J. *Faraday Soc. Trans.* **1971**, *67*, 2251.
(29) Theoretical Physical Chemistry TU Darmstadt Home Page. http://www.theo.chemie.tu-darmstadt.de.
(30) Bicerano, J. *Prediction of Polymer Properties*, 2nd ed.; Marcel Dekker: New York, 1996.
(31) Karimi-Varzaneh H. A.; Carbone, P.; Balasubramanian, S.; Müller-Plathe, F. Unpublished work.
(32) Mognetti, B. M.; Yelash, L.; Virnau, P.; Paul, W.; Binder, K.; Müller, M.; MacDowell, L. G. *J. Chem. Phys.* **2008**, *128*, 104501.

MA801910R